# Equilibrium Unfolding of the C-Terminal SAM Domain of p73 †

**ARTICLE** *in* BIOCHEMISTRY · JUNE 2002

Impact Factor: 3.02 · DOI: 10.1021/bi0159478 · Source: PubMed



**4 AUTHORS**, INCLUDING:

Francisco N. Barrera
University of Tennessee
**44** PUBLICATIONS **655** CITATIONS

SEE PROFILE

# Equilibrium Unfolding of the C-Terminal SAM Domain of p73[†]

Francisco N. Barrera, María T. Garzón, Javier Gómez, and José L. Neira*

*Centro de Biología Molecular y Celular, Universidad Miguel Hernández, 03202 Elche (Alicante), Spain*

*Received November 14, 2001; Revised Manuscript Received January 31, 2002*

ABSTRACT: The sterile alpha motif (SAM) domain is a protein module of approximately 65 to 70 amino acids found in many diverse proteins whose functions range from signal transduction to transcriptional repression. The alpha splice variant of p73 (p73 α), a homologue of the tumor suppressor p53, has close to its C-terminus a SAM motif. Here, we report the folding equilibrium properties of the p73 α SAM domain (SAMp73) by using different biophysical techniques (circular dichroism, fluorescence, and Fourier transform infrared spectroscopies, and differential scanning calorimetry). Those probes indicate that SAMp73 folds via a two-state mechanism. Fluorescence experiments performed at different pHs showed two titrations: the first one due to an acid residue (with a p$K_a$ = 4.5 ± 0.3) and the second due to deprotonation of tyrosine residues. The conformational stability of the protein upon chemical denaturation was determined over the pH range 3 to 10. The maximum conformational stability is $\Delta G = 5.7 \pm 0.4$ kcal mol$^{-1}$ (at 25 °C) and occurs in a broad maximum, with little variation, between pH 6 and 10. The high melting temperature of SAMp73 ($T_m$ = 93.5 °C), despite its moderate conformational stability at 25 °C, can be ascribed to its low heat capacity change upon unfolding, $\Delta C_p$, which is estimated to be around 915 cal K$^{-1}$ mol$^{-1}$ at 25 °C and only around 543 cal K$^{-1}$ mol$^{-1}$ at the $T_m$. The implications of the temperature-dependent nature of $\Delta C_p$ are discussed in relation to the thermal stability of proteins as opposed to their conformational stability at room temperature.

p53 is a key tumor suppressor preventing the genetic malignant alterations in cells. This protein is a modular molecule with a transcriptional activation domain, DNA-binding domain, and oligomerization domain, which mediates tetramerization. The products of two cloned genes, p73 (*1*, *2*) and p63 (*3*), share strong sequence homology with the different domains of p53. For instance, p73 shares 63% identity with the DNA-binding region of p53 (including the conservation of all DNA contact residues), 38% identity with the tetramerization domain, and 29% with the transactivation domain. Conversely to human p53, p73 contains an additional C-terminal extension. This extension is subject to alternative splicing, which results in six terminal variants (p73 α−$\phi$) (*1*, *4*). These splice variants have different transcription and biological properties; thus, it seems that the C-terminal region is responsible for the differences observed among the variants. For example, p73 $\beta$ transactivates many p53-responsive promoters, and p73 α does so at a lesser extent (*2*, *5*, *6*). However, both variants of p73 promote apoptosis irrespective of the p53 status (*1*) and suppress apoptosis focus formation (*2*, *4*). Furthermore, p73 α and $\beta$ proteins are upregulated in p53-deficient tumor cells in response to overexpressed oncogenes; it seems that, in the absence of p53, oncogenes can activate p73 to induce apoptosis in tumor cells (*7*).

The p73 α variant has close to its C-terminus a SAM[1] domain, which is thought to be responsible for regulating p53-like functions (*8*). The structure of this SAM domain, SAMp73, has been resolved by NMR (*9*) and X-ray crystallography (*10*, *11*). The domain (residues 487−554 of the full p73 protein) contains a Cys−XX−Cys motif and a single tryptophan residue, which could be used as a probe to monitor the conformational changes in the protein under various conditions. The structure of the domain reveals a small five-helix bundle composed of four α-helices [residues 491−499 (helix 1), 506−511 (helix 2), 525−531 (helix 3) and 538−550 (helix 5)], and a small $3_{10}$-helix (residues 517−520). It has been noted that the SAMp73 domain has a structural similarity with two ephrin receptors tyrosine kinases (*9*); furthermore, the spatial arrangement of the bundle is similar to the SAM domains found in other proteins (*12*). This domain is putatively considered to be responsible for regulating protein functions via self-association or by association with other SAM domains (*13*), but its exact function is not known. The crystal structure reveals a dimeric organization, but the NMR structure is monomeric (*9*),

[†] This work was supported by Project from Generalitat Valenciana GV-00−024−5 and Project BIO2000−1081, from the Spanish Ministerio de Ciencia y Tecnología. F.N.B. was recipient of a predoctoral fellowship from Generalitat Valenciana.

* Corresponding author address: José L. Neira, Centro de Biología Molecular y Celular, Edificio Torregaitán, Universidad Miguel Hernández, Avda del Ferrocarril s/n, 03202, Elche (Alicante), Spain. Tel: + 34 966658459. Fax: + 34 966658758. E-mail: jlneira@umh.es

[1] Abbreviations: ASA, solvent-accessible surface area; ANS, 1-anilinonaphthalene-8-sulfonic acid; CD, circular dichroism; $\Delta ASA_{total}$, the total solvent-accessible surface area exposed upon unfolding; DSC, differential scanning calorimetry; $\Delta C_p$, heat capacity change; $\Delta H_{cal}$ the calorimetric enthalpy change; $\Delta H_{VH}$, van't Hoff enthalpy change; FTIR, Fourier transform infrared; GdmCl, guanidinium hydrochloride; NMR, nuclear magnetic resonance; RNase, ribonuclease; SAM, sterile alpha motif; SAMp73, the C-terminal region of the p73 protein comprising residues 487−554 of the intact protein; $T_m$, thermal denaturation midpoint; UV, ultraviolet.

10.1021/bi0159478 CCC: $22.00 
Published on Web 04/12/2002

suggesting that the dimer formation in the crystal is an effect of crystal packing rather than a real physiological state; furthermore, sedimentation experiments have shown that SAMp73 is monomeric, under a wide range of experimental conditions (*9*, and unpublished results).

Because of its small size (67-residues long), we are using SAMp73 as a model for folding, stability, and binding studies. We have embarked in the study of the stability of this domain, and how its stability is affected by the presence of denaturants and other macromolecules, to get insights into its function and how it can mediate in cancer mechanisms. We aim to design mutants of SAMp73 involved in cancer development to study whether there is a relationship between stability and malignancy. To do so, we need to know in depth the determinants of the stability of the mutant and wild-type proteins. Our findings in this work show that SAMp73 wild-type is moderately stable over a wide pH range, reaching its maximum stability in the range pH 6 to 10, and that the protein folds via a two-state folding mechanism. The thermodynamical parameters obtained from DSC experiments indicate a high thermal midpoint denaturation, $T_m$. The overall picture obtained from both chemical- and heat-induced denaturation studies is consistent with a moderately stable protein at 25 °C, although it is highly resistant toward thermal unfolding. The implications of the temperature-dependent nature of $\Delta C_p$ are discussed in relation to the thermal stability of proteins as opposed to their conformational stability at 25 °C. To our knowledge, this study represents the first report characterizing the equilibrium unfolding of a SAM domain, and one of the first folding studies on proteins involved in tumor suppression and regulation (*14*, *15*).

## EXPERIMENTAL PROCEDURES

*Materials.* Urea and GdmCl ultrapure were from ICN Biochemicals. GdmCl molecular biology grade was from Sigma. Exact concentrations of urea and GdmCl were calculated from the refractive index of the solution (*16*). Imidazole, Trizma base, NaCl, and ANS were from Sigma. $\beta$-Mercaptoethanol was from BioRad, and the $Ni^{2+}$-resin was from Invitrogen. Dialysis tubing was from Spectrapore with a molecular weight cutoff of 3500 Da. Standard suppliers were used for all other chemicals. Water was deionized and purified on a Millipore system.

*Protein Expression and Purification*. The SAMp73 clone, comprising residues 487−554 of the intact p73 and a $His_6$-tag at the N terminus, was kindly donated by C. H. Arrowsmith. We have carried out all the studies with this construction since its structure is well-known by NMR (*9*) and no differences were observed with that obtained by X-ray, where the $His_6$-tag was removed (*10*, *11*). Recombinant protein was expressed in *Escherichia coli* C43 strain (*17*), and purified using $Ni^{2+}$ chromatography. To eliminate any protein or DNA bound to the resin, coeluting with the protein, an additional gel filtration chromatography step was carried out by using a Superdex 75 16/60 gel filtration column (Amersham Pharmacia Biotech). The yield was 30−35 mg of protein *per* 1 L of culture. The samples were dialyzed extensively against 0.2 M NaCl, lyophilized, and stored at −80 °C. Samples for unfolding studies were prepared by dissolving the lyophilized protein in deionized water (unfolding) or in 7 M GdmCl (in the experiments to test the folding reversibility). Protein concentration was calculated from the absorbance of stock solution measured at 280 nm, using the extinction coefficients of model compounds (*18*).

*Fluorescence Measurements.* All fluorescence spectra were collected on a SLM 8000 spectrofluorometer (Spectronics Instruments, Urbana, IL), interfaced with a Haake water bath, at 25 °C, in all cases. Sample concentration was in the range 2−6 $\mu$M, and the final concentration of the buffer was, in all cases, 10 mM. A 0.5-cm-path-length quartz cell (Hellma) was used.

(*a*) *Steady-State Fluorescence Measurements.* The protein samples were excited at 280 and at 295 nm in the pH range 3−12 to characterize a possible different behavior of tryptophan or tyrosine residues (*19*). GdmCl unfolding experiments were acquired by excitation at 280 nm, because no differences were observed between the excitation either at 280 nm or at 295 nm (data not shown). The slit width was typically equal to 4 nm for the excitation light, and 8 nm for the emission light. The fluorescence experiments were recorded between 300 and 400 nm. The signal was acquired for 1 s and the increment of wavelength was set to 1 nm. Blank corrections were made in all spectra.

The GdmCl titrations, either followed by fluorescence or CD, were carried out by dilution of the proper amount of the 7 M denaturant stock solution and leaving the samples at 25 °C, for at least 3 h prior to performing the experiments. No differences were observed between the samples prepared the previous night and those prepared 3 h before acquisition. As the concentration of GdmCl was increased, the fluorescence spectra were red-shifted and their intensities were increased (data not shown).

In the pH-induced unfolding experiments, either followed by fluorescence or CD, the pH was measured after completion of the experiments, and essentially no differences were observed with those pHs calculated from the buffer stock solutions. The pH was measured with an ultrathin Aldrich electrode in a Radiometer (Copenhagen) pH meter. The pH range explored using both techniques was 2 to 12. The salts and acids used in buffer preparation were pH 2.0−3.0, phosphoric acid; pH 3.0−4.0, formic acid; pH 4.0−5.5, acetic acid; pH 6.0−7.0, $NaH_2PO_4$; pH 7.5−9.0, Tris acid; pH 9.5−11.0, $Na_2CO_3$; pH 11.5−13.0, $Na_3PO_4$.

(*b*) *Fluorescence Quenching Experiments.* Quenching of intrinsic tryptophan fluorescence by iodide or acrylamide (*20*) was examined at different pHs. Excitation was at 280 nm (for quenching of tyrosine and tryptophan residues) and 295 nm (for quenching of the tryptophan residue); emission was measured from 300 to 400 nm. In experiments employing KI as a quencher, ionic strength was kept constant by addition of KCl; also, $Na_2S_2O_3$ was added to a final concentration of 0.1 M to avoid formation of $I_3^-$. The slit width was set at 8 nm for both excitation and emission. The dynamic and static quenching constants for acrylamide were obtained by fitting the data from different wavelengths (in the range 330−340 nm) to the Stern−Volmer equation, which includes an exponential term to account for static quenching (*20*):

$$F_0/F = 1 + K_{sv}[X]^{(v[X])} \quad (1)$$

where $K_{sv}$ is the Stern−Volmer constant for collisional

quenching and $v$ is the static quenching constant. Similar values of $K_{sv}$ and $v$ were obtained at the above indicated wavelengths (data not shown). Iodide quenching did not show a significant static component, and then the exponential term was not included in the fitting of eq 1. In both quenchers, the range of concentrations explored was 0−0.7 M.

(*c*) *ANS Binding.* ANS binding was detected by collecting fluorescence spectra at different pHs in the presence of 50 $\mu$M dye. Excitation wavelength was 380 nm, and emission was measured from 400 to 600 nm. Slit widths were 4 nm for excitation and 8 nm for emission. Stock solutions of ANS were prepared in water and diluted into the samples to the above final concentration. In all cases, all the blank solutions were subtracted from the corresponding spectra.

*Circular Dichroism Measurements*. Circular dichroism spectra were collected on a Jasco J810 spectropolarimeter fitted with a thermostated cell holder and interfaced with a Neslab RTE−111 water bath. The instrument was periodically calibrated with (+) 10-camphorsulfonic acid. Isothermal wavelength spectra at different pHs were acquired at a scan speed of 50 nm/min with a response time of 2 s and averaged over four scans at 25 °C. Far-UV measurements were performed using 20−40 $\mu$M of protein in 10 mM buffer, using 0.1- or 0.2-cm-path length cells. Near-UV spectra were acquired using 30−40 $\mu$M of protein in a 0.5-cm-path length cell. All spectra were corrected by subtracting the proper baseline.

Thermal denaturation experiments were performed at constant heating rates of 30, 60, and 100 °C/h and a response time of 8 s. Thermal scans were collected in the far-UV region at 222 nm from 25 °C (or 5 °C) to 90 °C (or 95 °C) in 0.1-cm-path length cells with a total protein concentration of 20−40 $\mu$M. Thermal scans were collected in the near-UV region at 280 nm from 25 °C (or 5 °C) to 90 °C (or 95 °C) in 0.5-cm-path length cells with a total protein concentration of 40−50 $\mu$M. The solution conditions were the same as those reported in the steady-state far-UV experiments. The reversibility of thermal transitions was tested by recording a new scan after cooling to 5 or 10 °C the thermally denatured sample, and comparing it with the spectra obtained in the first scan. The possibility of drifting of the CD spectropolarimeter was tested by running two samples containing buffer, before and after the thermal experiments. No difference was observed between the scans. Every thermal denaturation experiment was repeated at least twice with new samples. In all cases, after the reheating experiment, the samples were transparent and no precipitation was observed.

In the GdmCl denaturation experiments, far-UV CD spectra were acquired at a scan speed of 50 nm/min, and four scans were recorded and averaged at 25 °C. The response time was 2 s. The path length cell was 0.1 cm, with a protein concentration of 20−40 $\mu$M in the far-UV CD experiments; for the near-UV CD experiments, the path length cell was 0.5 cm, with a protein concentration of 40−50 $\mu$M. Spectra were corrected by subtracting the baseline in all cases. The chemical denaturation reaction is fully reversible, as demonstrated by the sigmoidal curves obtained by starting from diluted 7 M GdmCl samples at different pHs (data not shown). Every chemical denaturation experiment was repeated at least three times with new samples.

*Analysis of the pH and Chemical Denaturation Curves, and Free Energy Determination*. The wavelength averaged emission intensity, $\langle\lambda\rangle$, in fluorescence spectra was calculated from (*21*):

$$\langle\lambda\rangle = \frac{\sum_1^n \frac{1}{\lambda_i} I_i}{\sum_1^n I_i} \quad (2)$$

where $I_i$ is the fluorescence intensity measured at a wavelength $\lambda_i$. This parameter was used to map the changes in the exposure of aromatic residues in the chemical and pH denaturation experiments.

The pH denaturation experiments were analyzed assuming that both species, protonated and deprotonated, contribute to the fluorescence spectrum:

$$X = \frac{(X_a + X_b 10^{(pH-pK_a)})}{(1 + 10^{(pH-pK_a)})} \quad (3)$$

where $X$ is the physical property being observed (ellipticity or fluorescence), $X_a$ is the physical property being observed at low pHs (that is, the fluorescence or ellipticity of the acid form), $X_b$ is the physical property observed at high pHs, and p$K_a$ is the apparent p$K$ of the titrating group. The apparent p$K_a$ reported was obtained from three different measurements, prepared with new samples.

To facilitate comparison among the different biophysical techniques, data were converted to the fraction of folded and unfolded molecules according to the expression:

$$f_N = \frac{(X - X_D)}{(X_N - X_D)} \quad (4)$$

where $X_N = \alpha_N + \beta_N[D]$ and $X_D = \alpha_D + \beta_D[D]$ are the corresponding fractions of the folded and unfolded states, respectively, for which a linear relationship with denaturant is usually assumed, and $X$ is the physical property (ellipticity or fluorescence) being observed. The majority of the data were obtained by following the ellipticity at 222 nm upon chemical denaturation. The denaturation data obtained by fluorescence or CD were fitted to the two-state equation:

$$X = (X_N + X_D e^{(-\Delta G/RT)})/(1 + e^{(-\Delta G/RT)}) \quad (5)$$

where $X_N$ and $X_D$ are the corresponding fractions of the folded (N) and unfolded states (U), respectively, which have been defined above, $R$ is the gas constant, and $T$ is the temperature in K.

Chemical denaturation curves at the different pHs were analyzed using a two-state unfolding mechanism, according to the linear extrapolation model: $\Delta G = m([D]_{50\%} - [D])$ (*16*), where $\Delta G$ is the free energy of denaturation, [D] is the denaturant concentration, and $[D]_{50\%}$ is the one at the midpoint of the transition. The chemical denaturation binding model (*22*, *23*) was also used for the fitting of the chemical denaturation data, but no reliable parameters were obtained for $\Delta G$ (data not shown). Thus, the linear free-energy model was used in all the conformational stability calculations.

Urea was used, as the first choice, in the chemical denaturation experiments to avoid any electrostatic effects caused by GdmCl. However, in most of the pHs explored, there were not enough points at high denaturant concentrations (the unfolding baseline), precluding a reliable determination of $m$ and $[\text{urea}]_{50\%}$ parameters. At low pHs, however, it was possible to determine those parameters, and a comparison was carried out with those obtained from the GdmCl denaturation experiments (see Discussion).

Fitting by nonlinear least-squares analysis to eqs 1, 3, and 5 was carried out by using the general curve fit option of Kaleidagraph (Abelbeck software) on a PC computer.

*Fourier Transform Infrared Spectroscopy.* The protein was lyophilized and dissolved in deuterated buffer Tris 10 mM and 0.3 M NaCl (pH 7.4). No corrections in the measured pH were done for the isotope effects. Samples of SAMp73 at a final concentration of 6 mg/mL were placed between a pair of $CaF_2$ windows separated by a 50 $\mu$m thick spacer in a Harrick Ossining demountable cell. Spectra were acquired on a Nicolet 520 instrument equipped with a deuterated triglycine sulfate detector and thermostated with a water bath at 25 °C. The cell container was continuously filled with dry air. Usually 600 scans/sample were taken, averaged, apodized with a Happ-Genzel function, and Fourier transformed to give a final resolution of 2 $cm^{-1}$. The contributions of buffer spectra were subtracted, and the resulting spectra were used for analysis after smoothing. The spectra smoothing was carried out applying the maximum entropy method (*24*). Derivation of FTIR spectra was performed using a power of 3 and a breakpoint of 0.3. Fourier self-deconvolution was performed using a Lorentzian bandwidth of 18 $cm^{-1}$ and a resolution enhancement factor of 2 (*25*). The prediction of protein secondary structure quantified by deconvolution of the amide I band (*24*) yielded essentially the same percentage of α-helix, $\beta$-turns, and random-coil structure than that observed in the high-resolution NMR (*9*) and X-ray (*10*, *11*) structures (data not shown).

Thermal denaturation experiments followed by FTIR were also done at a protein concentration of 6 mg/mL, 0.3 M NaCl with a scanning rate of 50 °C/h, and acquired every 5 °C.

*Differential Scanning Calorimetry*. DSC experiments were performed with a MicroCal MC-2 differential scanning calorimeter interfaced to a computer equipped with a Data Translation DT-2801 A/D converter board for instrument control and automatic data collection. Lyophilized protein was dissolved in buffer (10 mM MES buffer, 0.2 M NaCl, pH 6.5) and dialyzed extensively (twice) against 2 L of the same buffer at 4 °C. Since the protein unfolds irreversibly when heated at concentrations above 1 mg/mL (data not shown, and see results), all calorimetric experiments were performed at concentrations below 0.5 mg/mL. Samples were degassed under vacuum for 10 min with gentle stirring prior to being loaded into the calorimetric cell. Samples were heated at a constant scan rate of 60 °C/h and held under a constant external pressure of 1 bar to avoid both bubble formation and evaporation at temperatures above 95 °C. Before the samples were rescanned, they were cooled in situ to 20 °C for 40 min. Experimental data were corrected from small mismatches between the two cells by subtracting a buffer vs buffer baseline, prior to data analysis. After normalizing to concentration, a chemical baseline calculated from the progress of the unfolding transition was subtracted.

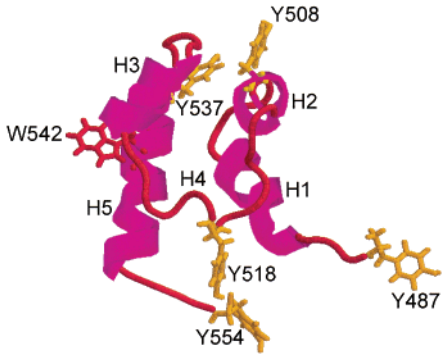


FIGURE 1: Structure of SAMp73: NMR structure of SAMp73 (*9*), showing the aromatic side chains of the protein. The nomenclature of the helices are H1: residues 491−499; H2: 506−511; H4: 517−520 (the $3_{10}$ helix); H3: 525−531; H5: 538−550. The figure was produced with Rasmol (*52*).

The excess heat capacity functions were then analyzed using the software package Origin (Microcal Software, Inc.).

## RESULTS

*pH-Induced Unfolding Experiments.* To examine how the secondary and tertiary structures of SAMp73 change by pH, we used multiple spectroscopic techniques (*26*), which give complementary information about the melting of the secondary and/or tertiary structure of the protein.

(*a*) *Fluorescence Experiments.* We have used fluorescence to map any change in the tertiary structure of the protein upon pH changes (*19*). SAMp73 has one tryptophan and five tyrosine residues. Trp542, in the numbering of intact p73, is in the middle of the last helix (the fifth helix) forming the hydrophobic core of the protein (Figure 1). Tyr487 is at the beginning of the domain; Tyr508 is in the middle of second helix; Tyr518 and Tyr537 are at the beginning of helix 4 and helix 5, respectively; the last tyrosine, Tyr554, is the C-terminal residue, and it is following to Asp553. The emission fluorescence spectrum of native SAMp73 has a maximum at 335 nm at low and neutral pHs; thus, it is dominated by the emission of the sole tryptophan residue. As the pH increases above neutral pH, the maxima of the spectra are red-shifted toward 345 nm, probably due to basic unfolding.

We examined fluorescence spectra using the $\langle\lambda\rangle$ parameter obtained by excitation at two different wavelengths (280 and 295 nm) (Figure 2). The profile of $\langle\lambda\rangle$ upon excitation at 280 nm versus pH shows two titrations at low and at high pH. We could not determine the $pK_a$ of the titration at high pH because of the absence of the baseline at basic pHs. This titration is concomitant with the red shift of the spectra at high pHs, and because of its high $pK_a$, it seems to be related with the deprotonation of the Tyr residues (*27*). Conversely, the apparent $pK_a$ of the titration at low pH is 4.5 ± 0.3 (determined by using eq 3 in the pH range 2 to 7). This value is close to that of the side chains of Glu, Asp, and/or the C-terminal residues (*27*).

Conversely, the fluorescence spectra obtained when excited at 295 nm did not show any titration either at low or high pH (Figure 2, inset). Since at 295 nm Trp542 is preferentially excited, these facts suggest that both titrations, observed upon excitation at 280 nm, might involve tyrosine residues.

(*b*) *ANS Binding*. ANS binding was used to monitor the extent of exposure of protein hydrophobic regions, and to

Table 1: Quenching Constants for SAMp73 in Acrylamide and KI[a]

| | acrylamide | | | | KI | |
|---|---|---|---|---|---|---|
| | 280 | | 295 | | 280 | 295 |
| conditions | $K_{sv}$ ($M^{-1}$) | $v$ ($M^{-1}$) | $K_{sv}$ ($M^{-1}$) | $v$ ($M^{-1}$) | $K_{sv}$ ($M^{-1}$) | $K_{sv}$ ($M^{-1}$) |
| pH 1.8 | $9.9 \pm 1.5$ | $2.4 \pm 0.2$ | $5.1 \pm 0.3$ | $0.6 \pm 0.1$ | $1.02 \pm 0.07$ | $2.3 \pm 0.3$ |
| pH 6.3 | $8.6 \pm 0.2$ | $2.59 \pm 0.03$ | $5.1 \pm 0.5$ | $0.5 \pm 0.2$ | $1.7 \pm 0.1$ | $2.3 \pm 0.2$ |
| pH 11.9 | $6.4 \pm 0.3$ | $2.69 \pm 0.07$ | $3.1 \pm 0.3$ | $0.8 \pm 0.2$ | $1.52 \pm 0.06$ | $1.7 \pm 0.1$ |
| 5 M GdmCl | $15.0 \pm 2.0$ | $3.1 \pm 0.2$ | $6.7 \pm 0.5$ | $0.4 \pm 0.1$ | $3.6 \pm 0.1$ | $5.9 \pm 0.8$ |

[a] Errors are data fit errors to eq 1 with (acrylamide) or without (KI) exponential factor. The constants were obtained by fitting of fluorescence intensity at 338 nm vs concentration of quenching agent (similar constants were obtained by fitting the intensities at 335, 336, and 337 nm, data not shown). Experiments were carried out at 25 °C. The experiments at 5 M GdmCl were carried out at pH 6.

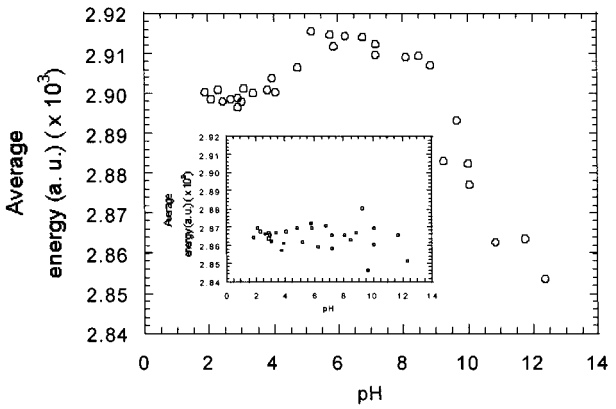


FIGURE 2: pH-induced unfolding of SAMp73 followed by fluorescence: The average energy is represented versus the pH by excitation at 280 nm. Inset: The average energy obtained at each pH by excitation at 295 nm. The conditions were 6 $\mu$M of protein, 0.2 M NaCl at 25 ($\pm$ 0.1) °C; buffer concentration was 10 mM in all cases; spectra were acquired in 0.5-cm-path-length cells.

detect the existence of non-native partially folded conformations, upon pH-induced unfolding (*28*, *29*). All the spectra showed maxima at 480 nm, with no large changes in the fluorescence intensity (data not shown) in the whole pH range, suggesting that no exposure of any hydrophobic region was occurring.

(*c*) *Examination of Tryptophan Exposure by Fluorescence Quenching*. To further check whether the tertiary structure around the Trp changes upon pH, we examined iodide and acrylamide quenching by excitation at 295 nm. In the structure of SAMp73 (Figure 1), Trp542 is partially shielded from the solvent; thus, if any partial unfolding occurs as pH changes, the accessibility of the tryptophan should change. Excitation at 280 nm was also carried out to test for the accessibility of tyrosine residues.

Acrylamide-quenching experiments with excitation at 295 nm yielded exponential Stern−Volmer plots. The $K_{sv}$ parameter remains constant, within the error, at acid and neutral pHs, but decreases at basic pHs (Table 1). This indicates that at low pHs, the solvent exposure of Trp542 does not change significantly; conversely, at high pHs, the exposure of Trp542 changes probably because of basic unfolding. Quenching control experiments in the presence of 5 M GdmCl (pH 6), where the protein is completely unfolded (data not shown), yielded larger $K_{sv}$ than those observed at any pH (Table 1), suggesting a complete exposure of Trp542 to the solvent. The $v$ parameter did not change substantially either at high [GdmCl] or pH. The behavior of the acrylamide $K_{sv}$, upon excitation at 280 nm, follows the same pattern than that observed at 295 nm. The obtained $v$ parameters are the same, within the error, at any pH, and slightly larger at 5 M GdmCl. In general, both parameters, $K_{sv}$ and $v$, are larger, using the acrylamide quencher, when excited at 280 nm than at 295 (Table 1), reflecting the fact that at 280 nm, tyrosine and tryptophan are excited.

The use of KI yielded similar results at both excitation wavelengths: the $K_{sv}$ remain nearly the same at low and neutral pHs, and decreases slightly at basic pHs. The small variation observed at low pHs, when excited at 280 nm, could be due to partial decomposition of $Na_2S_2O_3$, which is known to be unstable at acid pHs (*30*); its decomposition would lead to the formation of $I_3^-$, which absorbs strongly at 280 nm. At high [GdmCl], the $K_{sv}$ increases, as it does in acrylamide. Conversely to that observed in acrylamide, there are no large differences between those $K_{sv}$ measured at 280 or 295 nm. The reasons of this behavior are not known, but they could be either due to the large volume of acrylamide when compared to KI, or to the fact that the iodide has a negative charge.

(*d*) *Far- and Near-UV CD Experiments.* We used far-UV CD in the analysis of the unfolding of SAMp73 as a spectroscopic probe that is sensitive to protein secondary structure (*31*, *32*). Its CD spectrum is very intense and has the features of an $\alpha$-helical protein, with minima at 222 and 208 nm (data not shown), although interference from the aromatic residues cannot be ruled out at 222 nm (*31*, *32*). This shape did not change over the pH range explored, suggesting that secondary structure is not altered significantly (data not shown). No residual ellipticity was present when the protein was denatured by GdmCl.

We used near-UV CD to detect for possible changes in the asymmetric environment of aromatic residues (*31*, *32*). The near-UV of SAMp73 is very weak, and there are not intense bands, despite the presence of a large number of aromatic residues. No significant residual ellipticity was detected when the protein was denatured at high [GdmCl]. The near-UV spectrum does not change with the pH (data not shown), indicating that the changes observed in fluorescence upon pH did not alter significantly the asymmetric environment of the aromatic residues.

In conclusion, all spectroscopic probes indicate that SAMp73 maintains essentially its secondary and tertiary structure between pH 2 and 12. At high pHs, evidence of basic unfolding is observed in the fluorescence spectra, and thus, in the tertiary structure.

*Thermal Denaturation Experiments.* To obtain the thermodynamical parameters characterizing the unfolding transition of SAMp73, we carried out thermal denaturation experiments.

(*a*) *Far- and Near-UV CD Experiments.* We explored the thermal denaturation behavior of SAMp73 in the 2.5−11.7 pH range (data not shown). The thermal profiles did not show a baseline at the higher temperatures, except at pH 11.7. At this pH, a sigmoidal behavior was obtained, but the thermal midpoint could not be determined from the thermal measurements because of the irreversibility of the process. At lower pHs, SAMp73 seems to unfold reversibly, as concluded from the coincidence of the heating and reheating curves. Unfortunately, the high $T_m$ (> 90 °C) precluded its accurate determination (data not shown).

To decrease the $T_m$, we assayed the acquisition of thermal experiments in the presence of different [GdmCl]. Extrapolation of these melting temperatures at 0 M GdmCl should allow us to obtain a reliable measurement of the $T_m$. The [GdmCl] assayed at pH 6 were 0.2, 0.4, 1, 1.4, and 1.8, where the protein is fully folded (data not shown). In all cases, the protein unfolded reversibly, as indicated by the superposition of the heating and reheating curves. However, the $T_m$ could not be determined either because the transitions were not very steep or they did not show a large enough baseline at low or high temperatures.

Thermal denaturation experiments followed by near-UV did not show a sigmoidal behavior either (data not shown).

(*b*) *FTIR Experiments.* FTIR is a powerful method for investigation of protein secondary structure. The main advantage in comparison with CD and fluorescence is that FTIR is much more sensitive to the presence of $\beta$-structure or random-coil. Upon heating, the shape of the amide I band of SAMp73 changed dramatically (Figure 3 A), with: (i) a substantial loss in the integrated intensity of bands arising from α-helix; and (ii) the appearance of a strong band at 1620 $cm^{-1}$, and a weaker band at 1680 $cm^{-1}$, which correspond to interactions between extended chains, and have been related to aggregation of thermally unfolded proteins (*33*). The measure of the width at half-height upon temperature allowed us the characterization of the melting curve (Figure 3B). The melting transition resembles that obtained by CD experiments (data not shown). Again, no estimation of the thermodynamical parameters for the unfolding transition was possible due to the high $T_m$.

The FTIR thermal denaturation experiments were not reversible, when the sample was cooled and reheated (data not shown). These findings agree with the results found by DSC (see below), where at high protein concentrations (at 1−2 mg/mL) SAMp73 seems to aggregate upon heating.

(*c*) *DSC Experiments.* To get further insights about the energetics involved in the folding equilibrium of SAMp73, we studied the heat-induced denaturation of the protein by DSC. Due to the high melting temperature, $T_m$, suggested by CD and FTIR thermal denaturation studies, the protein was scanned up to 115 °C (close to the upper limit of temperature operation of the instrument). The reversibility of the unfolding transition was tested by rescanning the samples under the same experimental conditions. The level of reversibility of the transition was found to be strongly concentration-dependent. At concentrations in the range of 1−2 mg/mL, the protein unfolds irreversibly due to aggregation (data not shown), and the DSC endotherm is highly scan-rate dependent. It is clear that, under these conditions, the unfolding reaction is under kinetic control, and, therefore, no thermodynamic information can be extracted from the DSC experiments (since the reaction is not under equilibrium). The level of reversibility of the heat-induced unfolding of the protein increased as protein concentration decreased.

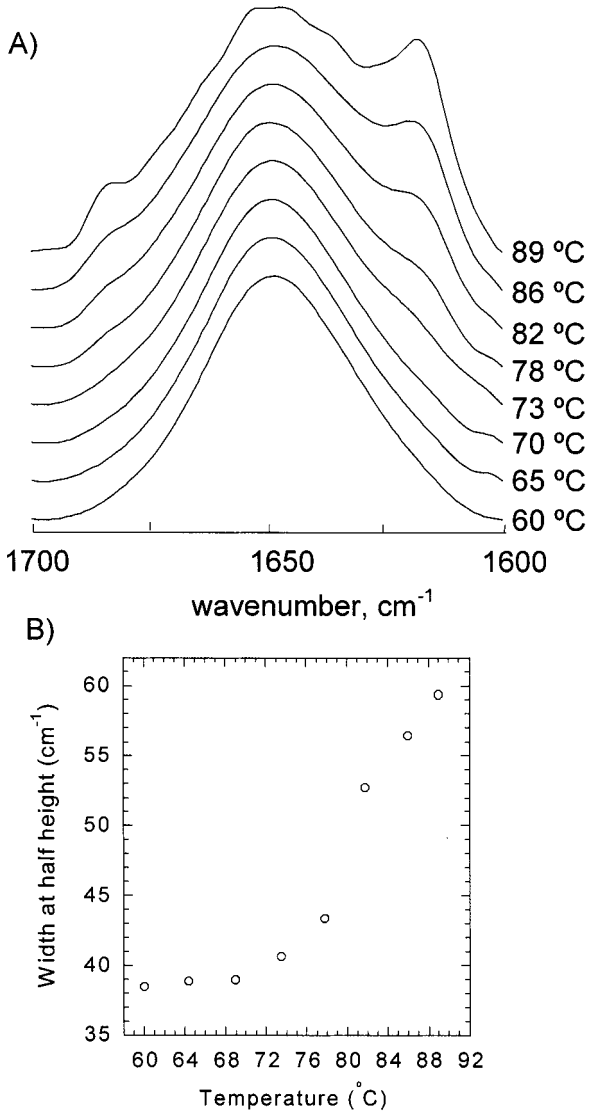


FIGURE 3: Thermal denaturation profiles followed by FTIR: (A) Thermal denaturation profiles of SAMp73 at pH = 7.4. (B) Thermal behavior of SAMp73 followed by the width at the half-height of the amide I band. The conditions were 6 mg/mL of protein, 0.3 M NaCl; buffer concentration was 10 mM.

At concentrations below 0.5 mg/mL (65 $\mu$M), no scan rate dependence was detected for the thermodynamic parameters extracted from the excess heat capacity function. However, a significant decrease in the calorimetric molar enthalpy was detected upon rescanning the sample, proving that a fraction of the protein was unable to fold after the first scan, probably due to the high temperatures used in the DSC experiments (115 °C). Nevertheless, both the excess heat capacity function for the scan and rescan experiments were consistent with the two-state reversible model and led to virtually the same melting temperatures, $T_m$, and van't Hoff enthalpies, $\Delta H_{VH}$.

The results in Figure 4 confirm the extremely high thermal stability of the protein previously observed in the CD and FTIR thermal denaturation experiments. For scan A, the $T_m$ was 93.5 ± 0.1 °C, and the calorimetric enthalpy change upon denaturation of the protein, $\Delta H_{cal}$, was 59.8 ± 0.4 kcal $mol^{-1}$. The van't Hoff to calorimetric enthalpy ratio, $\Delta H_{VH}$/

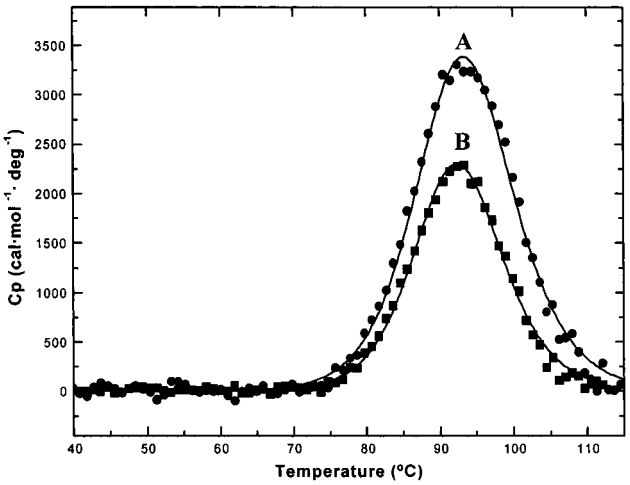


FIGURE 4: DSC measurements of SAMp73: Excess heat capacity function of SAMp73 at pH 6.5 in 10 mM MES buffer containing 0.2 M NaCl. The protein (0.45 mg/mL, 58 $\mu$M) was heated at a constant scanning rate (60 °C/h) up to 115 °C (scan A), cooled, and reheated under identical conditions (scan B). The continuous lines represent the fitting of the experimental data to a two-state reversible model. The melting temperature, $T_m$, was 93.5 ± 0.1 °C for scan A and 92.6 ± 0.1 °C for scan B (rescan). For scan A, the calorimetric enthalpy change upon denaturation of the protein, $\Delta H_{cal}$, was 59.8 ± 0.4 kcal mol$^{-1}$ and the van't Hoff to calorimetric enthalpy ratio, $\Delta H_{VH}/\Delta H_{cal}$, was 1.01. $\Delta H_{cal}$ for scan B was around 62% of the one obtained for scan A indicating that a portion of the protein was irreversibly unfolded after being heated at 115 °C (see text).

$\Delta H_{cal}$, was 1.01, suggesting that no stable intermediate is significantly populated as the native state unfolds to give raise to the denatured state ensemble of the protein. The excess heat capacity function of the protein obtained in the rescan (scan B) is also consistent with a two-state reversible model. Both the $T_m$ and the $\Delta H_{VH}$ are virtually identical to those obtained in scan A (92.7 °C and 61.2 kcal mol$^{-1}$, respectively). A significant decrease in the calorimetric enthalpy change (37.2 kcal mol$^{-1}$) is observed when compared to that obtained in the first scan (59.8 kcal mol$^{-1}$), indicating that around 38% of the protein (at this concentration, 0.45 mg/mL) was unable to fold when cooled after being heated to 115 °C.

The situation described above can be explained in terms of the Lummry-Eyring model in which the equilibrium between the native and unfolded states of the protein (N and U, respectively), given by the equilibrium constant, *K*, is coupled with some kind of irreversible transformation (with a *k* kinetic constant) of the unfolded state yielding the irreversible denatured state, D:

$$N \overset{K}{\rightleftharpoons} U \overset{k}{\rightarrow} D$$

The results shown in Figure 4 indicate that at concentrations below 0.5 mg/mL, the native and unfolded states of SAMp73 equilibrate rapidly in comparison to the time constant of the calorimeter (in the order of 20 s). The unfolding transition is under microequilibrium conditions, and the parameters derived from the excess heat capacity of the protein ($T_m$, $\Delta H_{cal}$ and $\Delta H_{VH}$) can be interpreted in terms of classical equilibrium thermodynamics. Conversely, as the concentration of protein is increased, being aggregation a multimolecular process, the kinetics of the irreversible process is

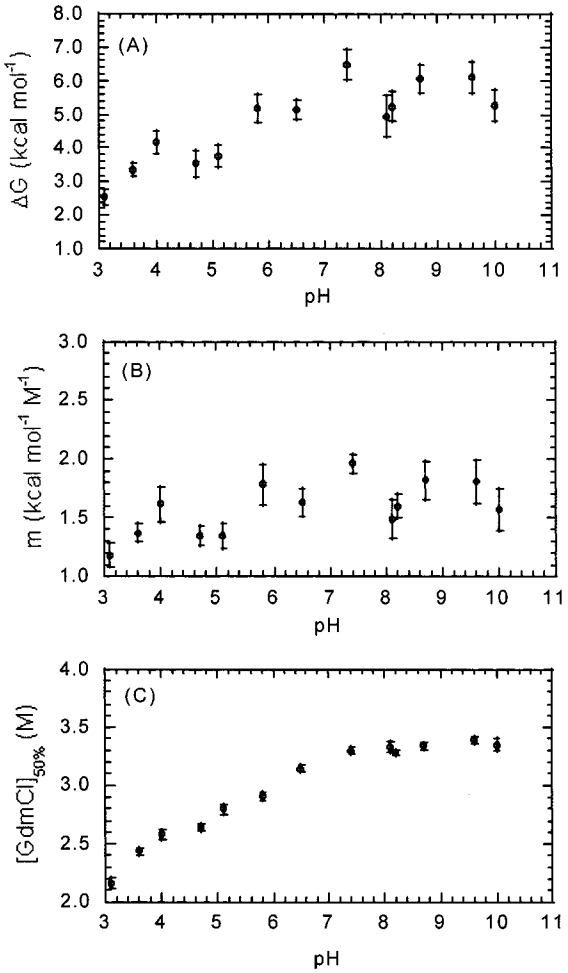


FIGURE 5: Stability of SAMp73: (A) Curve of stability with the pH of SAMp73 at 25 (± 0.1) °C, measured by CD GdmCl denaturation experiments. (B) Curve of the *m* values measured by CD GdmCl denaturation experiments. (C) The midpoints of the denaturation curves. The conditions were 20 $\mu$M of protein 0.2 M NaCl in both cases, at 25 (± 0.1) °C; buffer concentration was 10 mM in all cases. Spectra were acquired in 0.1-cm-path-length cells.

accelerated and the denaturation reaction monitored by DSC is no longer under microequilibrium.

It should be stressed here that the chemical- and thermal-equilibrium unfolding of SAMp73 is completely reversible under concentrations lower than 20 $\mu$M (data not shown, and Figure 5). Only at high protein concentrations (as those used in the DSC and FTIR experiments), there is evidence of irreversibility probably because of protein aggregation and the high temperatures used.

*Free Energy Profile as a Function of pH.* The free energy profile of SAMp73 was obtained by measurements of chemical denaturation at any pH (Figure 5), by following the ellipticity at 222 nm. The chemical denaturation process is completely reversible at the different pHs, as shown by the superposition of the chemical denaturation experiments started from the fully folded and unfolded protein (data not shown). The unfolding process follows a two-state folding mechanism, as concluded from the agreement of the denaturation curves followed by fluorescence and far-UV CD (see Discussion). SAMp73 is moderately stable at acid and neutral pHs. Its maximum conformational stability at 25 °C is $\Delta G$ = 5.7 ± 0.4 kcal mol$^{-1}$ (the average from the free energy values measured between pH 6 and 10), occurring in a broad

maximum, with little variation, between pH 6 and 10. The *m* values of the chemical denaturation are fairly constant, except at very low pHs (see Discussion), over all the pH range explored (Figure 5), with an average value of 1.6 ± 0.2 kcal mol$^{-1}$ M$^{-1}$.

## DISCUSSION

*Free Energy and Stability of SAMp73 upon pH*. SAM domains have been suggested to be involved in protein−protein interactions (*8*, *12*, *13*), and usually, the isolated domains are prone to aggregate. This is why it has been impossible to study, so far, their folding properties under any conditions. The SAMp73 domain is monomeric under all the pHs studied as checked by sedimentation equilibrium data (*9*, and unpublished results), and then, we have been able to carry out equilibrium unfolding experiments to test for its stability.

Figure 5 shows the pH-dependence of the Gibbs free-energy of SAMp73 at 25 °C. Its maximum conformational stability averages 5.7 ± 0.4 kcal mol$^{-1}$, and occurs as a broad maximum between pH 6 and 10. The variation of Δ*G* with pH is greatest around pH 3.5, suggesting that ∼1−2 protons are bound upon unfolding. At low pH where native SAMp73 is positively charged, the p*K*s of the carboxyl groups in the folded protein are expected to be lower than in the unfolded protein (*34*). Then, unfolded SAMp73 binds protons more tightly than folded SAMp73, and this seems to be the main reason in the stability decrease as the pH is lowered. Similar pH behavior has been observed in RNase A and RNase T (where the number of protons bound is nearly the same) (*35*, *36*), in barnase (*37*) and staphylococcal nuclease (*38*−*40*) (where the number of protons bound upon unfolding is ∼3−5).

Whether or not the *m* value depends on pH differs from protein to protein. In RNase A, a linear relationship was found (*35*), but a more complex behavior has been observed in RNase T1 (*35*), barnase (*37*), and staphylococcal nuclease (*39*, *40*). Recently, it has been suggested, by using a theoretical model, that either a decrease or increase in the *m* value when pH decreases, is related with the p$K_a$ values of a putative conformational intermediate (*40*). In SAMp73, the *m* value (Figure 5B) seems to be constant, within the experimental error, in all the pH range, except at very low pHs (pH 3), where a slight decrease is observed. According to this model (*40*), the decreasing would mean that the intermediate should have unfolded-like p$K_a$'s. Criteria used to ascertain two-state folding behavior (that is, no conformational intermediate involved) are: (i) coincidence of equilibrium denaturation transitions monitored by different probes (for example, fluorescence and CD); (ii) the agreement among the Δ*G* obtained from GdmCl and temperature denaturation with the Δ*G* from urea denaturation curves; (iii) the fitting to the two-state is better, as judged by statistical analysis, than that to the three-state model; (iv) the equivalence of the calorimetric and van't Hoff enthalpies; and (v) the requirement that the unfolding free energy and its denaturant-dependence from equilibrium denaturation experiments is identical to that obtained from kinetics of folding and refolding (*41*). In SAMp73, we have found that chemical denaturation transitions monitored by fluorescence and CD are identical at pH 3.9 (data not shown), where a low *m* value could be observed (Figure 5B). Also, we have observed that the free energies from urea and GdmCl denaturation experiments are the same within the error (for instance, at pH 2.8, where a transition with large enough baselines at low and high [urea] could be obtained, yielded: $\Delta G = 2.7 \pm 0.2$ vs $2.5 \pm 0.3$ kcal mol$^{-1}$ obtained at pH 3.1 in GdmCl); further, the fittings to the two-state model were statistically better than those obtained by using the three-state model (data not shown); and finally the ratio $\Delta H_{VH}/\Delta H_{cal}$, obtained from the DSC studies, is close to 1 (see Results). Thus, it seems that the decrease of the *m* value at low pHs is not associated with the presence of an intermediate in SAMp73, and that this parameter is constant, within the error, at any pH. Rather, the low *m* value observed at pH 3 could be probably due to the absence of a large baseline at low [GdmCl] (data not shown). The *m* value is 1.6 ± 0.2 kcal mol$^{-1}$ M$^{-1}$ (averaging all the values in Figure 5B, except that of pH 3). This value is higher than that obtained by multiplying the number of helical residues in SAMp73 (39 residues, from the NMR structure, (*9*)) and the *per* residue *m* value for helix unfolding (0.023 kcal mol$^{-1}$ M$^{-1}$) (*42*): 0.897 kcal mol$^{-1}$ M$^{-1}$. Caution must be taken, however, because the above *per*-residue parameter was obtained from model peptides using urea as the chemical denaturant (*42*). An *m* value can also be estimated from the linear relationship between *m* and $\Delta ASA_{total}$ (*43*):

$$m \text{ (cal mol}^{-1}\text{ M}^{-1}) = (368 + 0.11\ \Delta ASA_{total}) \quad (6)$$

The $\Delta ASA_{total}$ from the NMR structure (*9*) is 5211.3 Å$^2$. The above expression yields 0.941 kcal mol$^{-1}$ M$^{-1}$, which is also slightly lower than that observed experimentally. Similar differences in the predicted and measured *m* values have been observed in other all-helical proteins (*44*), although the differences are smaller.

From the above results, it can be concluded that SAMp73 folds via a two-state mechanism, which is not surprising for a protein of that size, as it has been reported recently (*45*). On the other hand, it has been reported that there is a general tendency for proteins that denature at higher temperatures to have higher free energies of maximal stability (*46*). This is not the case in SAMp73; it has a small free energy of maximal stability and a very high thermal midpoint. This high $T_m$ is not associated either to any significant structural change with the pH (see below) or to changes in the free energy (see before), which is constant in a broad pH range. Thus, the reasons of that high thermal midpoint must rely on another thermodynamical parameter, rather than on Δ*G*.

*pH-Induced Unfolding of SAMp73*. The tertiary and secondary structure of SAMp73 does not change significantly between pH 3 and pH 12 as concluded from the fluorescence, CD, and ANS binding measurements. Neither is the number of solvent-exposed tyrosine or tryptophan as the pH increases, as concluded from the iodide and acrylamide experiments. The $K_{sv}$ quenching constants are similar to those observed in other proteins under native conditions: in glycyl tRNA synthetase the $K_{sv}$ is 0.35 ± 0.05 (in KI quenching, by excitation at 290 nm) (*47*), or the $K_{sv}$ in human serum albumin is 6.0 (in acrylamide by excitation at 290 nm) (*48*).

Also, the quenching parameters in the presence of 5 M GdmCl, where SAMp73 is completely unfolded (data not shown), are larger (Table 1) than those measured in native conditions, and similar to those observed in other proteins, for the completely unfolded state (*47*, *48*).

There are, however, small changes observed by fluorescence, at high and low pH. The changes at high pH are probably due to basic unfolding, as concluded from the presence of tyrosinate moieties (in the UV and FTIR experiments at high pH, the characteristic bands of those groups appear, data not shown). The change at low pH, consistent with the protonation of groups with an apparent $pK_a = 4.5 \pm 0.3$, is associated with the environment of one or several tyrosine residues, since the titration is only detectable upon excitation at 280 nm (Figure 2). The tyrosine residue closer to an acid residue is Tyr554, the C-terminal residue, and also the following residue to Asp553. Thus, it is tempting to suggest that the changes in fluorescence are related to this residue.

*Conformational Stability versus High Thermal Midpoints in SAMp73.* From the results presented above, it can be seen that, although the conformational stability of SAMp73 at 25 °C is not very high ($\Delta G = 5.7 \pm 0.4$ kcal mol$^{-1}$), the protein shows a remarkable stability upon thermal denaturation ($T_m$ = 93.5 °C). This behavior can be explained by the temperature dependence of $\Delta G$, which is given by the heat capacity change upon unfolding, $\Delta C_p$.

It has been shown (*49*) that the partial molar heat capacity, $C_p$, of a given conformational state of a protein in solution can be considered as composed of an intrinsic term (with contributions from covalent bonds and noncovalent internal interactions) and another term due to hydration (water−protein interactions). The molar heat capacity change, $\Delta C_p$, for the transition between two conformational states, A and B, of the protein can be calculated as $\Delta C_p = C_{p,B} - C_{p,A}$. Since the contribution arising from the covalent bonds is the same for all the conformational states of the protein, then $\Delta C_p$ is comprised only of the other two main contributions. These contributions can be rationalized in terms of the changes in accessible surface area (polar and nonpolar) and the total area upon unfolding (*49*, *50*). Taking into account the changes in solvent-accessible surface areas of SAMp73 upon unfolding, calculated from its NMR three-dimensional structure (*9*) ($\Delta ASA_{apolar} = 3239$ Å$^2$, $\Delta ASA_{polar} = 2125$ Å$^2$), together with the changes in the total buried surface area ($\Delta BSA_{total} = 5211$ Å$^2$), the temperature-dependent heat capacity change upon unfolding is given by (*49*):

$$\Delta C_p(T) = 915.1 - 1.937(T - 25) - 0.051(T - 25)^2 \quad (7)$$

where $T$ is given in °C and $\Delta C_p(T)$ in cal K$^{-1}$ mol$^{-1}$. According to eq 7 (Figure 6), the unfolding of SAMp73 is characterized by a rather low heat capacity change at 25 °C (915 cal K$^{-1}$ mol$^{-1}$) which monotonically decreases as temperature increases reaching a value of 543 cal K$^{-1}$ mol$^{-1}$ at $T_m$ (93.5 °C).

The Gibbs free energy change upon protein unfolding at any temperature, $\Delta G(T)$, can be calculated from the enthalpy and entropy changes at $T_m$, $\Delta H(T_m)$ and $\Delta S(T_m)$, together with the heat capacity change, $\Delta C_p$, according to the expression:

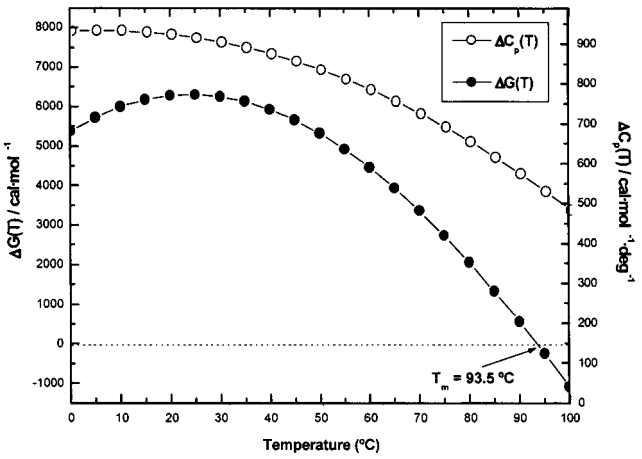


FIGURE 6: Calculated temperature dependence of the $\Delta C_p(T)$ and $(\Delta)G$ changes upon SAMp73 unfolding: The molar heat capacity change for the unfolding of SAMp73, $\Delta C_p(T)$, was calculated from the changes in accessible surface area of the protein induced by the conformational transition according to the model previously reported (*49*) using the NMR structure of the protein (*9*). $\Delta C_p(T)$ is strongly temperature-dependent going through a maximum at around 10 °C (933 cal K$^{-1}$ mol$^{-1}$) and decreasing monotonically as temperature is increased reaching a value of 543 cal K$^{-1}$ mol$^{-1}$ at $T_m$. The thermodynamical parameters characterizing SAMp73 unfolding at $T_m$ ($\Delta H(T_m) = 59.8$ kcal mol$^{-1}$ and $\Delta S(T_m) = 163.1$ cal K$^{-1}$ mol$^{-1}$) together with the calculated temperature-dependent $\Delta C_p$ were used to generate the $\Delta G$ versus temperature profile. The conformational stability of the protein at 25 °C was estimated in the order of 6.2 kcal mol$^{-1}$ in close agreement with the experimentally determined one (5.7 ± 0.4 kcal mol$^{-1}$).

$$\Delta G(T) = \Delta H(T) - T\Delta S(T) = \Delta H(T_m) + \int_{T_m}^{T} \Delta C_p dT - T\Delta S(T_m) - T\cdot\int_{T_m}^{T} \frac{\Delta C_p}{T} dT \quad (8)$$

Figure 6 shows the Gibbs free energy change for the unfolding of SAMp73 in the range 0−100 °C, calculated according to eq 8, and using the heat capacity function given by eq 7 and the thermodynamical parameters at $T_m$ obtained in the DSC studies ($\Delta H(T_m) = 59.8$ kcal mol$^{-1}$ and $\Delta S(T_m) = 163.1$ cal K$^{-1}$ mol$^{-1}$). The conformational stability of the protein at 25 °C estimated from the $\Delta G$ versus $T$ profile was 6.2 kcal mol$^{-1}$, in close agreement with the experimentally determined (5.7 ± 0.4 kcal mol$^{-1}$). The agreement between both values, and the fact that $\Delta G$ obtained from urea and GdmCl at low pHs (see above) is nearly the same, is suggesting that electrostatic contributions to the stability of SAMp73 are not very important.

These results unravel the mechanism of stabilization of SAMp73 toward thermal denaturation. While the protein is only moderately stable at 25 °C (close to the temperature of maximal stability, $T_{max} = 24.1$ °C), our experimental data indicate that the protein is surprisingly stable toward heat-induced denaturation ($T_m = 93.5$ °C). It seems clear from Figure 6 that this behavior is consistent with a rather small heat capacity change upon unfolding (915 cal K$^{-1}$ mol$^{-1}$ at 25 °C) that significantly decreases as the temperature is increased (543 cal K$^{-1}$ mol$^{-1}$ at $T_m$). The thermal stability of a protein can be attained either by a large maximum in

the $\Delta G$, $\Delta G_{max}$, or by a low $\Delta C_p$ (or by both reasons together); either factor makes the free energy curve intercept the *x*-axis (the *T* in Figure 6) at very high values. In SAMp73, the intercept with the *x*-axis is very high not because of the large stability of the protein (that is, not because there is a large $\Delta G_{max}$), but because of the very low $\Delta C_p$, which decreases with temperature (that is the higher the temperature, the lower the $\Delta C_p$). Thus, SAMp73 does not follow the general tendency observed in the thermostability for other proteins (*46*), because the $\Delta C_p$ changes with temperature. Similar explanations have been suggested to account for the high values of $T_m$ in hyperthermophilic proteins (*46*).

Some general conclusions can be extracted from the results presented here when designing protein mutants with increased thermal stability, as it is the case in many biotechnological applications. As shown in Figure 6, the thermal stability of a protein depends on both its free energy change at the temperature of maximal stability, $\Delta G_{max}$, and the heat capacity function upon unfolding, $\Delta C_p$ ($T$), which defines its temperature dependence. Therefore, a rational design strategy intended to enhance the thermal stability of a protein can be oriented either to *increase* the intrinsic stability, $\Delta G$, of the protein at 25 °C or to *decrease* its heat capacity change upon denaturation. In some proteins, both factors together contribute to increase the thermostability of the proteins; for example, in an analysis of a thermostable RNase H, the protein does not only have a great $\Delta G_{max}$, but also has a small $\Delta C_p$, which yields a broad stability curve (*51*). According to the results discussed above, in SAMp73 it would be much more effective to decrease $\Delta C_p$ by a given percentage than to increase its $\Delta G$ by the same fraction to attain a high thermal stability. Since $\Delta C_p$ increases with the amount of nonpolar area being exposed upon unfolding (*49*, *50*), the thermal stability of the protein could be enhanced by conservative mutations designed to increase the ratio of polar to nonpolar area buried in the folded state, while keeping mostly unaffected the intrinsic stability of the protein. It will be interesting to find out in future studies whether mutants, which can change that ratio, have a smaller $\Delta C_p$ and a higher $T_m$. It will be also interesting to test whether those mutants are involved in tumor development.

In summary we have carried out, to our knowledge, the first studies regarding the conformational stability of a SAM domain. The structure of SAMp73 does not change substantially as the pH decreases or increases. SAMp73 is a moderately stable protein at 25 °C with high stability toward heat denaturation, which folds via a two-state mechanism.

## ACKNOWLEDGMENT

We deeply thank Prof. C. H. Arrowsmith for the kindly gift of the SAMp73 clone; Dr. A. Pineda-Lucena for helpful suggestions and advice; and Prof. Ernesto Freire for the calculations of the solvent-accessible surface area. We gratefully acknowledge Dr. José M. González-Ros, Dr. José A. Encinar, and Dr. José A. Poveda for helpful discussions; Celia Agulló for determining two of the GdmCl denaturation curves; Dr. Germán Rivas and Dr. Carlos A. Botello for performing the sedimentation equilibrium experiments; and May García and Javier Casanova for excellent technical assistance. We also thank the two anonymous reviewers for their thought-provoking comments.

## REFERENCES

1. Kaghad, M., Bonnet, H., Yang, A., Creancier, L., Biscan, J. C., Valent, A., Minty, A., Chalon, P., Lelias, J. M., Dumont X., Ferrara, P., McKeon, F., and Caput, D. (1997) *Cell 90*, 809−819.
2. Jost, C. A., Marin, M. C., and Kaelin, W. G. Jr (1997) *Nature 389*, 191−194.
3. Schmale, H., and Bamberger, C. (1997) *Oncogene 15*, 1363−1367.
4. De Laurenzi, V., Costanzo, A., Barcaroli, D., Terrinoni, A., Falco, M., Annicchiarico-Petruzzelli, M., Levero, M., Mellino G. (1998) *Exp. Med. 188*, 1763−1768.
5. Zhu, J., Jiang, J., Zhou, W., and Chen, X. (1998) *Cancer Res. 58*, 5 061−5065.
6. Di Como, C. J., Gaiddon, C., and Prives, C. (1999) *Mol. Cell Biol. 19*, 1438−1449.
7. Zaika, A., Irwin, M., Sansome, C., and Moll, U. M. (2001) *J. Biol. Chem. 276*, 11310−11316.
8. Bork, P., and Koonin, E. V. (1998) *Nat. Genet. 18*, 313−318.
9. Chi, S.-W., Ayed, A., and Arrowsmith, C. H. (1999) *EMBO J. 18*, 4438−4445.
10. Wang, W. K., Proctor, M. R., Buckle, A. M., Bycroft, M., and Chen, Y. W. (2000) *Acta Crystallogr. D 56*, 769−771.
11. Wang, W. K., Bycroft, M., Foster, N. W., Buckle, A. M., Fersht, A. R., Chen Y. W. (2001) *Acta Crystallogr. D 57*, 545−551.
12. Thanos, C. D., and Bowie, J. U. (1999) *Protein Sci. 8*, 1708−1710.
13. Schultz, J., Pointing, C. P., Hoffmann, K., and Bork, P. (1997) *Protein Sci. 6*, 249−253.
14. Bullock, A. N., Henckel, J., DeDecker, B. S., Johnson., C. M, Nikolova, P. V., Proctor, M. R., Lane, D. P., and Fersht, A. R. (1997) *Proc. Natl. Acad. Sci. U.S.A. 94*, 14338−14342.
15. Mateu. M. G., Sanchez del Pino, M. M., and Fersht, A. R. (1999) *Nat. Struct. Biol. 6*, 191−198.
16. Pace, C. N. (1986) *Methods Enzymol. 131*, 266−280.
17. Miroux, B., and Walker, J. E. (1996) *J. Mol. Biol. 260*, 289−298.
18. Pace, C. N., and Schmid, F. X. (1997) in *Protein Structure* (Creighton, T. E., Ed.) 2nd ed., pp 253−259, Oxford University Press, Oxford.
19. Schmid, F. X. (1997) in *Protein Structure* (Creighton, T. E., Ed.) 2nd ed., pp 261−297, Oxford University Press, Oxford.
20. Lakowicz, J. R. (1999) *Principles of Fluorescence Spectroscopy*, 2nd ed., Plenum Press, New York.
21. Royer C. A. (1995) in *Protein Stability and Folding* (Shirley, B. A., Ed.) pp 65−89, Humana Press, Towota, New Jersey.
22. Schellman, J. A. (1955) *Biopolymers 26*, 549−559.
23. Aune, K., and Tandford, C. (1969) *Biochemistry 8*, 4586−4590.
24. Echabe, I., Encinar, J. A. and Arrondo, J. L. R. (1997) *Biospectroscopy 3*, 469−475.
25. Moffat, D. J., and Mantsch, H. H. (1992) *Methods Enzymol. 210*, 192−200.
26. Eftink, M. R. (1995) *Methods Enzymol. 259*, 487−512.
27. Cantor, C. R., and Schimmel, P. R. (1980) *Biophysical Chemistry*, W. H. Freeman and Company, New York.
28. Fink, A. L. (1999) in *The Encyclopedia of Molecular Biology* (Creighton, T. E., Ed.) pp 140−142, John Wiley & Sons Inc, New York.
29. Semisotnov, G. V., Rodionova, N. A., Razgulyaev, O. I., Uversky, V. N., Gripas, A. F., and Gilmanshin, R. I. (1991) *Biopolymers 31*, 119−128.
30. Rubinson, J. F. and Rubinson, K. A. (1998) *Contemporary Chemical Analysis*, 5th ed., Prentice Hall, New Jersey.
31. Woody, R. W. (1995) *Methods Enzymol. 246*, 34−71.
32. Kelly, S. M., and Price, N. C. (2000) *Cur. Prot. and Peptide Sci. 1*, 349−384.
33. Fernandez-Ballester, G., Castresana, J., Arrondo, J. L. R., Ferragut, J. A., and Gonzalez-Ros, J. M. (1992) *Biochem. J. 288*, 421−426.
34. Tandford, C. (1968) *Adv. Protein Chem. 23*, 121−282.
35. Pace, C. N., Laurents, D. V., and Thomson, J. A. (1990) *Biochemistry 29*, 2564−2572.

36. Yao, M., and Bolen, D. W. (1995) *Biochemistry 34*, 3771−3781.
37. Pace, C. N., Laurents, D. V., and Erickson, R. E. (1992) *Biochemistry 31*, 2728−2734.
38. Ionescu, R. M., and Eftink, M. R. (1997) *Biochemistry 36*, 1129−1140.
39. Whitten, S. T., and Garcia-Moreno, E. B. (2000) *Biochemistry 39*, 14292−14304.
40. Whitten, S. T., Wooll, J. O., Razeghifard, R., Garcia-Moreno, E. B., and Hilser, V. J. (2001) *J. Mol. Biol. 309*, 1165−1175.
41. Jackson, S. E., and Fersht, A. R. (1991) *Biochemistry 30*, 10428−10435.
42. Scholtz, J. M., Barrick, D., York, E. J., Stewart, J. M., and Baldwin, R. L. (1995) *Proc. Natl. Acad. Sci. U.S.A. 92*, 185−189.
43. Myers, J. K., Pace, C. N., and Scholtz, J. M. (1995) *Protein Sci. 4*, 2138−2148.
44. Padmanabhan, S., Jimenez, M. A., Gonzalez, C., Sanz, J. M., Gimenez-Gallego, G., and Rico, M. (1997) *Biochemistry 36*, 6424−6436.
45. Jackson, S. E. (1998) *Fold. Des. 3*, R81−R91.
46. Rees, D. C., and Robertson, A. D. (2001) *Protein Sci. 10*, 1187−1194.
47. Dignam, J. D., Qu, X., and Cahire, J. B. (2001) *J. Biol. Chem. 276*, 4028−4037.
48. Muzammil, M., Kumar, Y., and Tayyab, S. (2000) *Proteins 40*, 29−38.
49. Gómez, J., Hilser, V. J., Xie, D., and Freire, E. (1995) *Proteins 22*, 404−412.
50. Gómez, J., and Freire, E. (1995) *J. Mol. Biol. 252*, 337−350.
51. Hollien, J., and Marqusee, S. (1999) *Biochemistry 38*, 3831−3836.
52. Sayle, R. A., and Milner-White, E. J. (1995) *Trends Biochem. Sci. 20*, 374−376.

BI0159478